

D isorder and the e ective M n-M n exchange interaction in G a_{1-x}M n_xA s diluted m agnetic sem iconductors

Antônio J. R. da Silva,¹ A . Fazzio,¹ Rainundo R . dos Santos,² and Luiz E . Oliveira³

¹ Instituto de F sica, Universidade de São Paulo, CP 66318, 05315-970, São Paulo SP, Brazil

² Instituto de F sica, Universidade Federal do Rio de Janeiro,
CP 68528, 21945-970 Rio de Janeiro RJ, Brazil

³ Instituto de F sica, Unicamp, CP 6165, 13083-970 Campinas SP, Brazil

(Dated: Version 1.84 { 23rd May 2019)

We perform a theoretical study, using *ab initio* total energy density-functional calculations, of the effects of disorder and M n - M n exchange interactions for G a_{1-x}M n_xA s diluted sem iconductors. For a 128 atom s supercell, we consider a variety of con gurations with 2, 3 and 4 M n atom s, which correspond to concentrations of 3.1%, 4.7%, and 6.3%, respectively. In this way, the disorder is intrinsically considered in the calculations. Using a Heisenberg Ham iltonian to map the m agnetic excitations, and *ab initio* total energy calculations, we obtain the e ective $J_n^{Mn Mn}$, from n (n = 1) all the way up to sixth (n = 6) neighbors. Calculated results show a clear dependence in the magnitudes of the $J_n^{Mn Mn}$ with the M n concentration x. Also, con gurational disorder and/or clustering e ects lead to large dispersions in the M n-M n exchange interactions, in the case of xed M n concentration. Moreover, theoretical results for the ground-state total energies for several con gurations indicate the importance of a proper consideration of disorder in treating tem perature and annealing e ects.

PACS numbers: 71.55.Eq, 75.30.Hx, 75.50.Pp

I. INTRODUCTION

The exciting possibilities of manipulating both the spin and the charge of the carriers in sem iconductors, in such a way that new devices may be designed, have brought a lot of attention to the study of diluted m agnetic sem iconductors (D M S) in the past ten years or so. Even though the D M S have been known for a long time,¹ it was the discovery of ferromagnetism in p-type (In,M n)A s system² that spurred the research in this eld. This was even more so after the successful growth of ferromagnetic (G a,M n)A s alloys.³ This latter system has become almost a paradigm in the eld of D M S m aterials. It has long been known that isolated M n_{Ga} substitutional impurities give rise to acceptor states around 0.1 eV above the top of the valence band. Thus, the M n atom s have a double functionality in the G a_{1-x}M n_xA s alloys: they provide both (i) the m agnetic moments, and (ii) holes to intermediate the interaction between them. This somewhat simplistic view is much more complex than it seems at first sight. Ferromagnetism in G a_{1-x}M n_xA s only occurs for large M n concentrations of a few percent. As a consequence, the acceptor levels form a band which, due to the rather localized character of the defect state, has a dispersion which is far from what would result from a free quasi-particle picture. Moreover, the intrinsic disorder coupled to this somewhat narrow band indicates that any theoretical description based on an e ective mass description should be viewed with caution. To further complicate the issue, in order to obtain the necessary high M n concentrations the growth tem peratures cannot be too high, which would cause a lot of defects to be present in the samples, like M n interstitials (M n_I) and arsenic antisites (A s_{Ga}). As a result, the critical tem per-

ature and hole concentration, as a function of M n composition, are crucially dependent on the details of growth conditions.^{4,5,6,7,8,9,10,11,12,13,14,15,16}

In view of all these facts, it would be important to have a way to estimate the M n-M n exchange interactions (i) with as few assumptions as possible, (ii) which would treat the host and the M n impurities at the same level of accuracy, and (iii) which would furthermore include the e ects of disorder. This approach of implicitly tracing out the holes degrees of freedom has been implemented in a variety of ways based on self-consistent m ethods. Van Schilfgaarde and M ryasov¹⁷ have performed calculations of total energies, within the atomic spheres approximation, to extract exchange couplings, J's, for specific (i.e., not randomly chosen) clusters of closely spaced M n ions; their results suggest a tendency of a decrease in J when more M n atom s are added to nearby sites. More recently, Xu et al.¹⁸ used mu n-tin orbitals to investigate the dependence of the exchange coupling with the M n-M n distance at much larger (8.3%) concentrations of M n atom s; they found a considerable scatter in the values of the exchange couplings. A tight-binding linear mu n-tin orbital m ethod has been used by Kudrovsk y et al.,¹⁹ together with the m agnetic force theorem to study two M n impurities in a supercell; by varying the number of atom s in the supercell, a dependence of the exchange couplings with the concentration was inferred.

In this work we perform large supercell total energy calculations, based on *ab initio* density functional theory (DFT) m ethods. Within this approach, we treat disorder con gurations in which the M n atom s randomly replace G a atom s. By considering two, three, and four M n atom s in a supercell with 128 atom s, we cover three M n concentrations, 3.1%, 4.7%, and 6.3%, and present results

for the effective exchange interactions, J_n^{Mn-Mn} , between two Mn atoms which are n -th neighbors in the Ga sublattice, with $1 \leq n \leq 6$. Also, in a few cases the Mn atoms are placed in predetermined positions, in order to compare the exchange coupling of two nearest-neighbor Mn atoms in the presence of other Mn atoms, placed at various separations. The present results indicate a clear decrease in the magnitudes of the J_n^{Mn-Mn} with the Mn concentration x ; from now on, the Mn-Mn superscript in J_n^{Mn-Mn} will be omitted, in order to simplify the notation.

The work is organized as follows. In Section II we provide a brief description of the calculational procedure used in the present study. Results and discussion are left for Section III, and Section IV summarizes our findings and conclusions.

II. CALCULATIONAL METHOD

We have performed total energy calculations based on the density-functional theory (DFT) within the generalized-gradient approximation (GGA) for the exchange-correlation potential, with the electron-ion interactions described using ultrasoft pseudopotentials.²⁰ A plane wave expansion up to 230 eV as implemented in the VASP code²¹ was used, together with a 128-atom fcc supercell and 4 L-points for the Brillouin zone sampling; these L-points are non-equivalent, due to the presence of Mn impurities. The positions of all atoms in the supercell were relaxed until all the forces components were smaller than 0.02 eV/Å. For a 128 atom supercell, we consider a variety of configurations with 2, 3 and 4 Mn atoms, corresponding to concentrations of 3.1%, 4.7%, and 6.3%, respectively. Since calculations for all possible disorder configurations with more than 2 Mn atoms per cell is prohibitively costly in terms of computer time, we have considered typical configurations, as generated through the Special Quasi-random Structures (SQS) algorithm.²² A configuration is generated by placing the Mn atoms at Ga sublattice sites (64 possible sites). We then calculate the pair correlation functions, up to the sixth-neighbor, given by:

$$g_m(r) = \frac{1}{64Z_m} \sum_{i,j}^X g_m(i;j) S_i S_j: \quad (1)$$

Here g_m is the m th-neighbor pair correlation function, Z_m is the number of m th-order neighbors to a site, $g_m(i;j)$ is 1 if sites i and j are m th-order neighbors, and zero otherwise; and S_i is a variable taking values 0, if site i is occupied by Ga, and 1 if it is occupied by Mn. For a perfectly random (R) distribution of Mn atoms, the pair correlation function does not depend on m , $g_m(R) = x^2$, where x is the Mn concentration. For a given configuration we calculate the deviation from randomness as

$$\chi^2 = \frac{1}{m} \sum_{i,j}^X (g_m(i;j) - g_m(R))^2: \quad (2)$$

The above quantity indicates how random the configuration is. We perform an exhaustive search over all possible configurations and choose to work with the ones with lowest χ^2 .

For each chosen disorder configuration, we adopt the following strategy within our DFT-GGA calculations. As an initial guess, we take all valence electrons of each Mn atom aligned with each other, corresponding to $S = 5/2$ as expected in a d^5 configuration, and calculate the total energies for this configuration, as well as for an increasing number of tipped Mn total spins. The energy differences with respect to the aligned states, E_n , are then described by an effective Heisenberg model with appropriate first-, second-, and so forth, up to sixth-nearest-neighbor Mn-Mn couplings, J_n ; $n = 1 \dots 6$; see Sec. III and Appendix for details. This procedure has been applied^{23,24} to the case of two Mn atoms in a supercell with 128 sites, and we were able to infer the dependence of the effective couplings with both the Mn-Mn distance and direction: We have found^{23,24} that J_n does not display the alternating sign characteristic of the RKKY interaction, so that the Mn moments are always ferromagnetically coupled.

One should notice that for two Mn atoms, if the spins are treated quantum mechanically the above mentioned energy difference corresponds to that between the state with total spin 5/2 and the singlet one, leading to $J_n^{(Q)} = E_n = 15$. If the spins are treated classically, $J_n^{(C)} = 2 E_n = 25$ and the two approaches are entirely equivalent, apart from an overall multiplicative factor of 1.2. For more than two Mn atoms, we consider classical spins and note that this approximation, though not capturing full details of the excitation spectra, is still able to provide overall trends of the low energy magnetic excitations for a finite number of spins.

As a final methodological comment, we note that we have checked for spin-orbit effects (in the case of two Mn atoms) through the projector augmented-wave (PAW) method²⁵, and found a change from 0.29 eV to 0.24 eV in the total energy difference between the excited antiferromagnetic and ground state ferromagnetic Mn-spin alignments. Although a systematic study in this sense would certainly be important, this is beyond the scope of the present study and we have chosen to ignore spin-orbit effects in the total energy calculations presented in this work. We believe this approximation would not alter the general conclusions of the present study.

III. RESULTS AND DISCUSSION

A. Two Mn atoms

Let us first discuss the case of two Mn substitutional atoms in the 128-site supercell. We considered all configurations corresponding to all inequivalent positions within the supercell, i.e., Mn-Mn distances varying from

Table I: Estimates for the effective exchange coupling, J_n , in meV, between n th-nearest-neighbor Mn spins, S_i and S_j , for different Mn concentrations, x . In the case of 2 Mn atom s ($x = 3.1\%$), J_n is unique for a given n . For 3 Mn atom s ($x = 4.7\%$) in a supercell with 128 sites, we have performed calculations for 10 different SQS disorder configurations, and J_n is given by the average over the configurations in which two Mn sites are n th-neighbors; the number of such configurations are shown in square brackets, and the error bars are calculated as standard deviation of averages. In the case of 4 Mn atom s ($x = 6.3\%$), we show the results for two configurations (see text); note that sometimes a specific configuration would not accommodate the pertinent J_n .

n	$x = 3.1\%$	$x = 4.7\%$	$x = 6.3\%$	$x = 6.3\%$
1	23.2	18.2	1.5 [7]	12.6
2	10.4	3.8	1.8 [4]	—
3	13.6	6.6	2.7 [7]	2.8
4	5.6	3.6	0.8 [4]	4.8
5	2.6	+0.4	0.7 [5]	+0.1
6	4.4	1.9	0.7 [2]	—

4.06 Å up to 11.48 Å. Our total energy results yield a Mn–Mn ferromagnetic ground state in all cases. The relevant Heisenberg Hamiltonian in this case is

$$H = \sum_{\langle i,j \rangle} J_{ij} S_i \cdot S_j; \quad (3)$$

for each relative position in the supercell, where, for the sake of comparison with the cases of three and four Mn atom s (see below), S is taken as a classical spin of magnitude $5/2$; n is a vector connecting n th-nearest-neighbor Mn atom s replacing G a atom s. The estimates for J_n thus obtained are displayed in the second column of Table I.

As previously noted,^{23,24} the resulting Mn–Mn ferromagnetic effective coupling in $G_{1-x}M_nA_xS$ is essentially mediated by the antiferromagnetic coupling of each Mn spin to the quasi-localized holes. Also, the observed non-monotonic behavior of J_n should be attributed to the anisotropic character of the effective interaction. Moreover, J_n essentially decreases^{23,24} with Mn–Mn separation and vanishes above 10 Å.

B. Three Mn atom s

In the case of three Mn atom s in a supercell with 128 sites, we have performed calculations for 10 different disorder configurations. Figure 1 shows two SQS illustrative configurations: in (a) the 3 Mn atom s are somewhat clustered together, whereas in (b) two are nearest neighbors and the third is farther apart.

For each disorder configuration, the relevant Heisenberg Hamiltonian must contemplate the possibility of interactions occurring not only amongst spins within the supercell, but between one spin in the supercell and the different images in neighboring supercells (periodic boundary conditions effects, PBCE's). In actual fact,

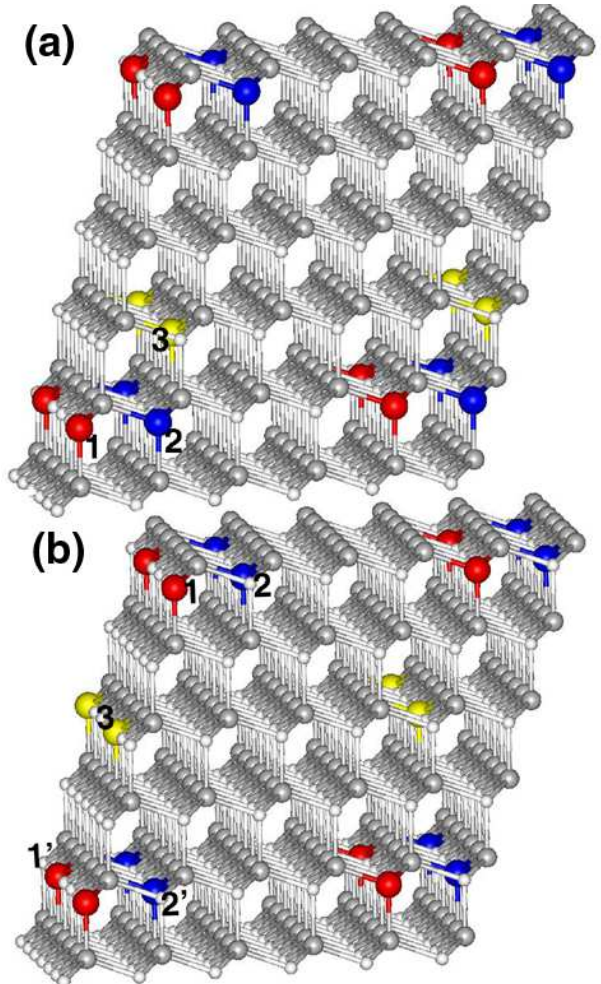


Figure 1: (Color online) A pictorial view of two possible realizations of disorder for three Mn atom s in a 128-site supercell ($x = 4.7\%$). Ga sites are represented by the smaller spheres, As sites by the middle-sized ones, and Mn atom s by the largest ones. For clarity, supercells are repeated along the different cartesian directions. The three nonequivalent Mn atom s are shown as different shades of gray (blue, red, and yellow in the color version).

depending on the disorder configuration, the same pair of spins may be j -th nearest neighbors within the supercell and k -th nearest neighbors when the images are considered. One can therefore write the Hamiltonian as

$$H = \sum_{\langle i,j \rangle} w_{ij}(n) J_n S_i \cdot S_j; \quad (4)$$

where the $w_{ij}(n)$ are geometrical weights taking into account PBCE's. For a given configuration, one expects most of the w 's to vanish; also, we set $w = 0$ if the distance between the Mn atom s is larger than 10 Å, as previously established.²⁴ In the Appendix we discuss the Hamiltonian for the two SQS configurations of Fig. 1. We then calculate the total energies for different Mn spin configurations: with all spins aligned, with only one spin reversed, either in site 1, 2, or 3, and so forth, increasing

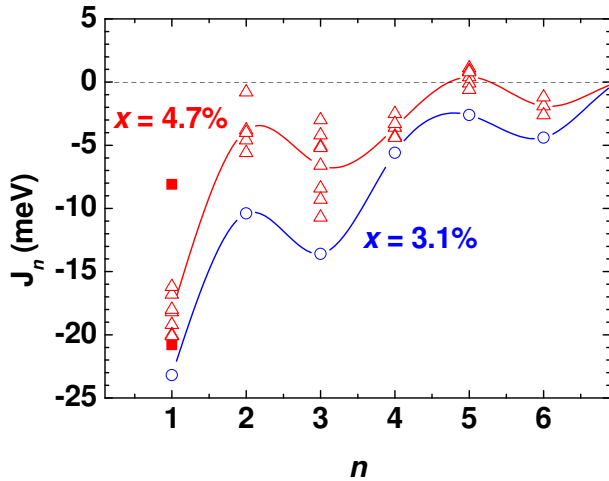


Figure 2: (Color online) The n th nearest-neighbor exchange coupling as a function of n for $x = 3.1\%$ and $x = 4.7\%$ (with data displayed for 10 SQ S configurations, see text). Full curves are guides to the eye (for $x = 4.7\%$ the full line goes through average values of J_n). Filled squares for J_1 correspond to extreme values obtained for the non-SQ S configurations; see text.

the number of spin sites, until one has the same number of unknowns (J_n) as equations (namely, the corresponding energy differences with respect to the aligned state).

It is instructive to lay out J_n as a function of n for the 10 SQ S realizations of disorder (three Mn atoms), as shown in Fig. 2; for comparison, we show the results for $x = 3.1\%$ in the same figure. One can see that the overall trend of J_n with n , observed in the case of two Mn spins, is maintained in this case, with the non-monotonic behavior still being due to effects of directionality. The corresponding average values of J_n , for each n , are shown in the third column of Table I. It is interesting to note that all J_n decrease (in absolute value) as the concentration of Mn atoms increases from 3.1% to 4.7%. While at first sight this may seem an unusual behavior, one should have in mind that the effective Mn-Mn interaction is hole-mediated, thus sensitive to the hole density.

In order to assess the effects of clustering in a systematic way, we have also considered non-SQ S configurations in which two Mn atoms are first neighbors, and a third Mn atom is placed in positions corresponding to fifth-, third-, and first-neighbor of the pair: we found that $J_1 = 20.8$ meV, 17.3 meV, and 8.1 meV, respectively; the extreme values are shown in Fig. 2 as filled squares. Thus, clustering tends to weaken the magnitude of the nearest-neighbor coupling. One may attribute this behavior as most likely resulting from the Coulomb repulsion between the holes, which leads to their delocalization as the Mn atoms group together, being therefore detrimental of their role as mediators of ferromagnetism.

If, on the one hand, clustering tends to decrease the magnitude of the nearest-neighbor exchange, on the other hand it leads to the energetically most stable configura-

Table II: Total energies from ferromagnetic SQ S configurations, labelled from 1 to 10, with respect to the total energy of the configuration corresponding to three nearest-neighbor Mn atoms clustered together.

n-th state	E_n (eV)	n-th state	E_n (eV)
1	0.054		
2	0.077		
3	0.085	8	0.158
4	0.090	9	0.176
5	0.091	10	0.227
6	0.103		
7	0.125		

tion. In Table II we display the energies of calculated ferromagnetic SQ S configurations relative to the clustered one in which the three Mn atoms are first-nearest neighbors. We note that the SQ S configurations labelled from 8 to 10, which have the highest total energies of the set, correspond to cases in which there are no first-neighbor pairs of Mn atoms. Since $Ga_{0.97}Mn_{0.03}As$ is only stable at growth temperatures in the range 200–300°C,^{6,26} the scale of energies shown in Table II indicates that not many configurations can be thermally activated. Clearly, there are several other mechanisms at play (such as mobility of Mn atoms, possibility of trapping on interstitials, and so forth), which are not included in the present approach, and will determine the final distribution of Mn atoms.

Figures 3(a)–(d) show the net magnetization $m(r) = \langle \mathbf{m} \rangle(r)$, where \mathbf{m} is the total charge density in the \pm -polarized channel, for three Mn atoms with all spins aligned and for only one tipped spin, for the configuration depicted in Fig. 1(a). Note that the densities on the upper right and upper left corners in each figure are related to a Mn atom and its image in a neighboring supercell. Similarly to the $m(r)$ of one²³ and two Mn impurities²⁴ in a supercell, near each Mn atom the local magnetization has a d-like character, whereas close to the As neighbors, the character changes to p-like, where $\mathbf{m} = (\mathbf{m}^+ \text{ or } \mathbf{m}^-)$ and $\mathbf{p} = (\mathbf{p}^+ \text{ or } \mathbf{p}^-)$. Also, $m(r)$ has a rather localized character. The tipping of spins introduce nodes on the $m(r)$ and subtle changes mostly on the orientation of the p-like lobes. Close to the Mn atoms, however, the local magnetization is not very sensitive to the tips.

C. Four Mn atoms

For four Mn atoms, we have considered only two disorder configurations, chosen according to the SQ S algorithm. A Hamiltonian similar to Eq. (4) may be written, with the addition of terms involving the fourth spin, having in mind that the interactions with spins on image sites are more frequent in this case.

For instance, in one of the calculated SQ S configura-

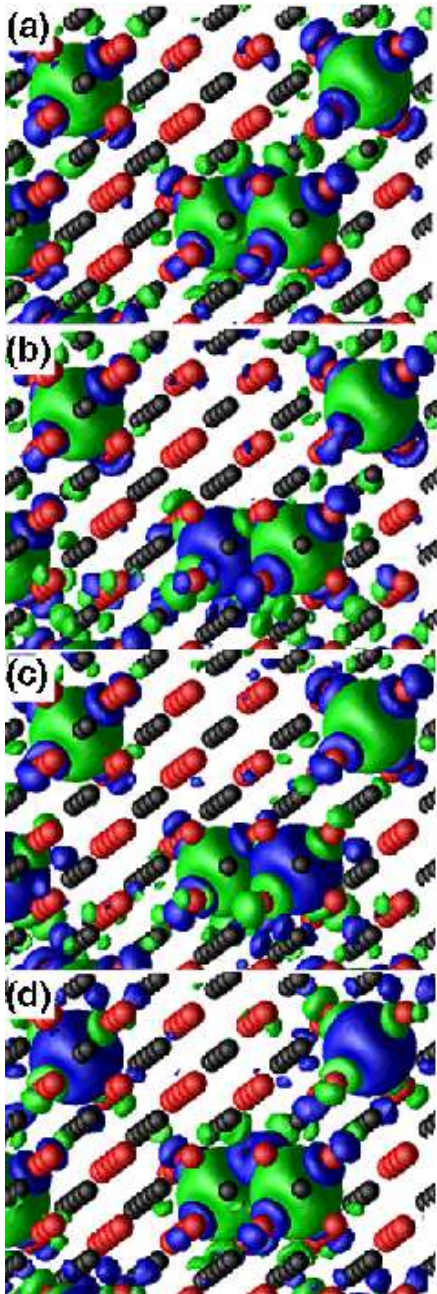


Figure 3: (Color online) Isosurfaces for the net local magnetization $m(r)$ (see text for definition) in the case of three Mn_{Ga} defects [for the configurations depicted in Fig. 1(a)], with (a) all spins aligned and (b)–(d) only one tipped spin. The green surface corresponds to a value of $+0.005 e\text{-}\text{\AA}^3$, and the blue surface to $-0.005 e\text{-}\text{\AA}^3$, with e being the electron charge. The black (red) spheres denote the Ga (Mn) atoms.

tions, the effective Hamiltonian becomes

$$H = 2J_5S_1 \cdot S + J_1S_1 \cdot S + J_3S_1 \cdot S + 2J_4S_2 \cdot S + J_3S_2 \cdot S + J_1S_3 \cdot S; \quad (5)$$

where the absence of a second-neighbor interaction should be noticed. Calculations of total energies for

all Mn spins parallel, and for the four possible single ips, lead to four excitation energies, from which the J_n 's ($n \leq 2$) may be inferred. A analogous considerations apply to the other SQ S con guration. The results are shown in columns 4 and 5 of Table I. One sees that the overall tendency of J_n is to decrease in magnitude as n is increased, in a pattern similar to that for smaller concentrations, though the dispersion cannot be properly assessed due to the scarcity of data. We also note that, as in the case of three Mn atoms, calculations with a non-SQ S con guration with the four Mn atoms clustered together indicate that clustering decreases the magnitude of the first-neighbor J_1 exchange coupling: $J_1 = 6.5$ m eV in this case, which should be compared with the 12.6 m eV and 13.0 m eV values of Table I.

D. The dependence of J_n with the concentration

The data in Table I can also be used to discuss the dependence of J_n with x , for a given n . In Fig. 4 we plot J_1 , J_2 , J_3 and J_4 as functions of x . For the case of J_1 , we also show (as filled symbols) three values obtained for the non-SQ S con gurations: two as mentioned before, in the case of three Mn atoms, and the one corresponding to four Mn atoms clustered together as first nearest-neighbors.

From Fig. 4, we see that, in most cases, the magnitudes of the exchange couplings decrease as the concentration of Mn atoms is increased. Further, this decrease may be quite significant; for instance, the magnitude of the average J_1 decreases by the order of 50% when one roughly doubles the concentration from 3.1%. We also see that for the con gurations in which the Mn atoms are clustered together, $|J_1|$ also decreases as x is increased. This overall decrease with x can be taken as numerical evidence that a steady increase in the concentration of Mn atoms is not sufficient to rise the critical temperature, since the exchange couplings will eventually be weakened. Clearly other effects may be playing important roles. For instance, within our present approach, the hole density is assumed to be the same as that of Mn atoms, which, as mentioned in the Introduction is not really the case. The presence of Mn interstitials and Mn - A s complexes also need to be taken into account in order to reach a quantitative agreement. Nonetheless, one expects that the trends unveiled here are indicative of the actual experimental situation.

IV. CONCLUSIONS

We have performed ab initio total energy density-functional calculations for two, three, and four substitutional Mn atoms in a 128 atoms supercell, corresponding to concentrations of 3.1%, 4.7%, and 6.3%, respectively. In this way, we have treated the host and the Mn impurities on equal footing. The effects of disorder have been

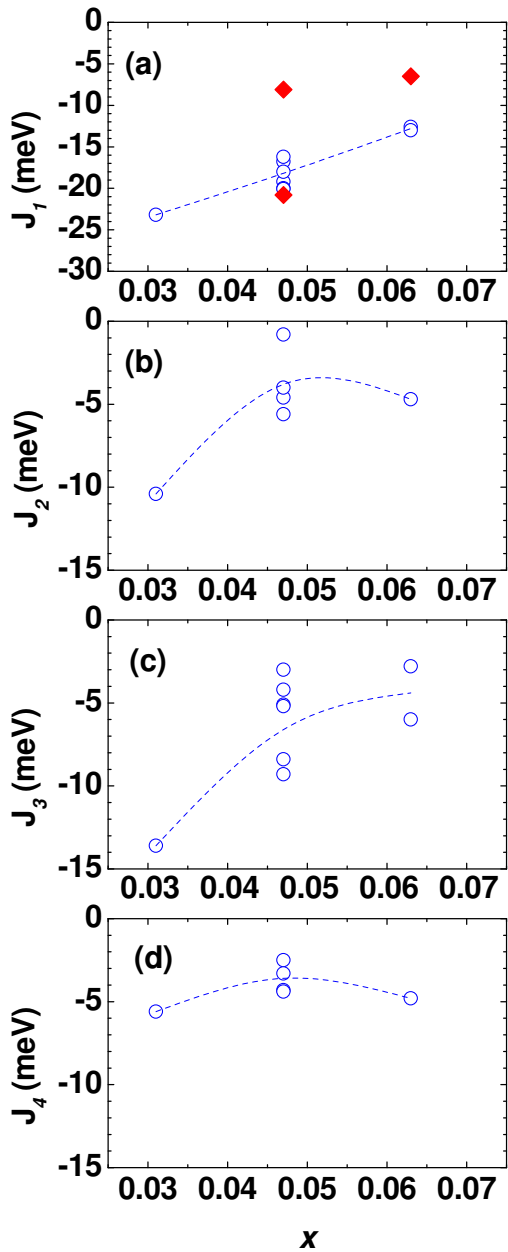


Figure 4: (Color online) Dependence of: (a) J_1 , (b) J_2 , (c) J_3 , and (d) J_4 with the concentration of Mn atoms. For $x = 3:1\%$, J_n is unique for a given n . Values for the SQS configurations are shown as empty circles, while the filled diamonds correspond to the extreme values obtained for the non-SQS configurations; see text. Dotted curves are guides to the eye through the average values of J_n .

assessed at different levels of approximations, depending on the concentration of Mn atoms: for $x = 3:1\%$, all possible non-equivalent positions of the Mn atoms have been considered; for $x = 4:7\%$, ten non-equivalent configurations have been generated through the SQS algorithm, while three specific ones have also been considered in order to discuss the effects of clustering; and, for $x = 6:3\%$, two SQS and one non-SQS configurations have been in-

vestigated. While the relation between the densities of holes and of Mn atoms is one of the yet unsolved issues in the context of DMS, here we have assumed that each Mn atom provides one hole; since our results relate to general trends, they may be carried over to the actual experimental situation of only a fraction of Mn atoms contributing with holes.

We have focused mainly on the effective exchange interaction between Mn spins, by mapping the spectra of magnetic excitations (spin gaps) onto a classical Heisenberg Hamiltonian with coupling constants J_n , ranging from first ($n = 1$) to sixth ($n = 6$) nearest neighbors. The effects of clustering on the nearest-neighbor pair-exchange coupling, J_1 , have been investigated by examining specific (i.e., non-random) configurations with three and four Mn atoms in the 128-site supercell. We have established that clustering tends to weaken the magnitude of the nearest-neighbor exchange coupling. On the other hand, we have found that clustered structures of Mn atoms have the lowest total energies, a result which may be of importance in a realistic discussion of annealing and/or diffusion effects. From calculations on random configurations we have also been able to determine the behavior of J_n with x , for fixed n : in most cases the exchange couplings get weaker as the concentration of Mn atoms is increased. This is consistent with the experimentally observed fact that there is an optimum range of Mn concentrations (whose quantitative determination requires a careful consideration of other disorder effects) in which the critical temperatures are the highest.

For fixed Mn density, we have found that the calculated J_n favor a ferromagnetic ground state, and have decreasing magnitude as the distance between spins increases (cf. Table I and Figs. 2 and 4). The non-monotonic behavior is attributed to directionality effects; by the same token, deviations in the sign of J_n were found only at large n ($= 5$), when its magnitude is already greatly reduced with respect to the nearest neighbor value. The discrepancy of the present results with respect to recent calculations by Xu et al.,¹⁸ may be attributed to the fact that their multiband calculations are not full potential; they therefore do not fully reproduce the crucial role played by the directional sp^3 bonds and by the hole p-states. Also, due to the quite significant variations of the calculated exchange couplings with configurations and Mn concentration, we emphasize that estimates of the critical temperature obtained via exchange couplings thus obtained are clearly open to question. We should also stress that the present results corroborate that the Mn-Mn ferromagnetic effective coupling in $Ga_1 \times Mn_xAs$ is mediated by localized holes leading to an antiferromagnetic (non-RKKY) coupling of each Mn spin, as previously noted,^{23,24} and recently confirmed experimentally.²⁷ Therefore, the inescapable conclusion is that the main feature of a conventional free-electron-like or perturbative RKKY interaction should be ruled out^{28,29} in the case of $Ga_1 \times Mn_xAs$.

As a final point, some comments regarding future per-

spectives are in order. From one side, investigations using a similar procedure as employed here (where the disorder is explicitly included) of how impurities, such as interstitial Mn and As anti-sites, alter the effective exchange interactions are relevant. For a given Mn configuration, it should be interesting to see how the results depend on the relative position of the defects. On the other hand, our results raise some questions whose answers are not completely trivial: (i) The fact that the effective exchange interactions change with the Mn configuration make it clear that the use of a Heisenberg model, at least a simple one where only pair-interactions are considered, should be viewed with caution. It is not obvious that extensions of the Heisenberg model to triplets or even larger cluster interactions will remedy this fact; (ii) The use of ab initio calculations has been very important in order to provide a correct picture of the electronic structure of these systems. One of its great merits is the possibility of obtaining model-free results. However, whenever one needs to make predictions about the critical temperature (T_c), models have to be used. For instance, from ab initio results one may extract effective exchange parameters, as in the present work, and then via mean field or more sophisticated methods, like Monte Carlo calculations, it is possible to calculate T_c . Two crucial steps in this procedure are questionable. The first one is the use of a Heisenberg model, as already mentioned. The other is the use of a small supercell approximation. Calculating the critical temperature via any effective methodology that is based on small supercell ab initio calculations, even if this effective approach allows the search of a large number of distinct configurations, has a great risk of being nonsense, since, as we have shown, the exchange interactions depend sensitively on the Mn distribution. The root of the above problems is the necessity of introducing a model hamiltonian in order to extract excited states of the system associated with spin excitations. A possible solution to this problem could be the use of a semiempirical hamiltonian with a tight-binding description for the host material coupled with a many-body, atomic-like description for the Mn atoms. The manyfold of low-energy states representing the different Mn spin orientations, that will be obtained upon diagonalization of such a hamiltonian⁷, will replace the states obtained via the effective (but questionable) Heisenberg hamiltonian.

Acknowledgments

Partial financial support by the Brazilian Agencies CNPq, CENAPAD-Campos, Rede Nacional de Materiais Nanoestruturados/CNPq, FAPESP, FAPERJ, and Millennium Institute for Nanosciences/MCT is gratefully acknowledged.

Appendix

Here we discuss the case of three Mn atoms, for the two disorder configurations displayed in Figs. 1(a) and 1(b), and chosen according to the SQS algorithm. For the configuration in Fig. 1(a), the Hamiltonian [see Eq. (4)] may be written, having in mind that the interactions with spins on image sites are to be taken into account, as

$$H = J_1 S_1 \pm J_3 S_2 \pm 4J_6 S_1 \pm \quad (A.1)$$

where the absence of second-neighbor, fourth-neighbor, and fifth-neighbor interactions should be noticed.

In a similar way, for the configuration in Fig. 1(b), the Hamiltonian is given by

$$H = J_3 S_1 \pm 2J_4 S_1 \pm 2J_5 S_2 \pm \quad (A.2)$$

where one notes the absence of first-neighbor, second-neighbor, and sixth-neighbor interactions.

One may perform DFT-GGA calculations, and obtain the total energies for SQS configurations with all Mn $S = 5/2$ atoms aligned with each other, as well as for an increasing number of tipped Mn total spins. The total-energy differences with respect to the aligned states, ΔE , may then be obtained via an effective classical Heisenberg model with appropriate J_n exchange couplings up to $n = 6$.

For the disorder configuration in Fig. 1(a), noticing that classically one has $S_i \pm = \frac{25}{4}$, it is straightforward to obtain, using eq. (A.1), for the total energies of configurations with appropriate tipping of Mn total spins

$$E_0 = \frac{25}{4} (+ J_1 + J_3 + 4J_6) \quad (A.3)$$

$$E_1^1 = \frac{25}{4} (- J_1 + J_3 - 4J_6) \quad (A.4)$$

$$E_1^2 = \frac{25}{4} (+ J_1 - J_3 + 4J_6) \quad (A.5)$$

$$E_1^3 = \frac{25}{4} (+ J_1 + J_3 - 4J_6); \quad (A.6)$$

where the lower index indicates the number of tipped spins (from $+5/2$ to $-5/2$), and the upper index labels which spin was tipped. The differences in corresponding Heisenberg energies are therefore

$$E_1^0 = \frac{25}{4} (2J_1 + 8J_6) \quad (A.7)$$

$$E_2^0 = \frac{25}{4} (2J_1 + 2J_3) \quad (A.8)$$

$$E_3^0 = \frac{25}{4} (2J_3 + 8J_6); \quad (A.9)$$

and one may thus obtain $J_1 = 16.2$ meV, $J_3 = 3.0$ meV, and $J_6 = 1.2$ meV from the calculated first principles differences in total energies, i.e., $E_1^0 = 264$ meV, $E_2^0 = 241$ meV, and $E_3^0 = 99$ meV.

¹ Semiconductor and Semimetals, vol. 25 (Academic, New York, 1988), edited by J. K. Furdyna and J. Kossut.

² H. Ohno, H. Muneoka, T. Penney, S. von Molnar, and L. L. Chang, *Phys. Rev. Lett.* **68**, 2664 (1992).

³ H. Ohno, A. Shen, F. Matsuura, A. Oiwa, A. Endo, S. Katsumoto, and Y. Iye, *Appl. Phys. Lett.* **69**, 363 (1996).

⁴ A. V. Esch, L. V. Bockstal, J. D. Boek, G. Verbaan, A. S. van Steenbergen, P. J. W. Elmann, B. Grietens, R. Boogaerts, F. Herlach, and G. Borghs, *Phys. Rev. B* **56**, 13103 (1997).

⁵ F. Matsuura, H. Ohno, A. Shen, and Y. Sugawara, *Phys. Rev. B* **57**, R2037 (1998).

⁶ H. Ohno, J. Magn. Magn. Mater. **200**, 110 (1999).

⁷ S. J. Potashnik, K. C. Ku, S. H. Chun, J. J. Berry, N. Samarth, and P. Schier, *Appl. Phys. Lett.* **79**, 1495 (2001).

⁸ K. W. Edmunds, K. Y. Wang, R. P. Campion, A. C. Neumann, C. T. Foxon, B. L. Gallagher, and P. C. Main, *Appl. Phys. Lett.* **81**, 3010 (2002).

⁹ M. J. Seong, S. H. Chun, H. M. Cheong, N. Samarth, and A. M. Ascarellas, *Phys. Rev. B* **66**, 033202 (2002).

¹⁰ H. Asklund, L. Iver, J. Kanski, and J. Sadowski, *Phys. Rev. B* **66**, 115319 (2002).

¹¹ K. M. Yu, W. Walukiewicz, T. Wójcik, I. Kuryliszyn, X. Liu, Y. Sasaki, and J. K. Furdyna, *Phys. Rev. B* **65**, 201303 (2002).

¹² K. M. Yu, W. Walukiewicz, T. Wójcik, W. L. Lim, X. Liu, Y. Sasaki, M. Dobrowolska, and J. K. Furdyna, *Appl. Phys. Lett.* **81**, 844 (2002).

¹³ S. J. Potashnik, K. C. Ku, R. Nahendiran, S. H. Chun, R. F. Wang, N. Samarth, and P. Schier, *Phys. Rev. B* **66**, 012408 (2002).

¹⁴ R. Moriya and H. Muneoka, *J. Appl. Phys.* **93**, 4603 (2002).

¹⁵ R. R. dos Santos, L. E. Oliveira, and J. d. Albuquerque e Castro, *J. Phys.: Cond. Matter* **14**, 3751 (2002).

¹⁶ R. R. dos Santos, J. d. Albuquerque e Castro, and L. E. Oliveira, *J. Appl. Phys.* **93**, 1845 (2003).

¹⁷ M. van Schilfgaarde and O. N. M. Ryasov, *Phys. Rev. B* **63**, 233205 (2001).

¹⁸ J. L. Xu, M. van Schilfgaarde, and G. D. Samolyuk, *Phys. Rev. Lett.* **94**, 097201 (2005).

¹⁹ J. Kudrnovsky, I. Turek, V. Drchal, F. Maka, P. Weinberger, and P. Bruno, *Phys. Rev. B* **69**, 115208 (2004).

²⁰ D. Vanderbilt, *Phys. Rev. B* **41**, 7892 (1990).

²¹ G. Kresse and J. Hafner, *Phys. Rev. B* **47**, R558 (1993).

²² S. H. Wei, L. G. Ferreira, J. E. Bernard, and A. Zunger, *Phys. Rev. B* **42**, 9622 (1990).

²³ A. J. R. da Silva, A. Fazzio, R. R. dos Santos, and L. E. Oliveira, *Physica B* **340-342**, 874 (2003).

²⁴ A. J. R. da Silva, A. Fazzio, R. R. dos Santos, and L. E. Oliveira, *J. Phys.: Cond. Matter* **16**, 8243 (2004).

²⁵ G. Kresse and D. Joubert, *Phys. Rev. B* **59**, 1758 (1999).

²⁶ A. H. Macdonald, P. Schier, and N. Samarth, *Nature Mater.* **4**, 195 (2005).

²⁷ V. F. Sapega, M. Moreno, M. Ramsteiner, L. Dameritz, and K. H. Ploog, *Phys. Rev. Lett.* **94**, 137401 (2005).

²⁸ D. J. Priour, Jr., E. H. Hwang, and S. Das Samanta, *Phys. Rev. Lett.* **92**, 117201 (2004).

²⁹ C. Timm and A. H. Macdonald, cond-mat/0405484 (2004).